THE JOURNAL OF PHYSICAL CHEMISTRY B
A JOURNAL OF THE AMERICAN CHEMICAL SOCIETY

pubs.acs.org/JPCB

Article

Three Reasons Why Aspartic Acid and Glutamic Acid Sequences Have a Surprisingly Different Influence on Mineralization

Published as part of The Journal of Physical Chemistry virtual special issue "125 Years of The Journal of Physical Chemistry".

Tobias Lemke, Moritz Edte, Denis Gebauer, and Christine Peter*

Cite This: *J. Phys. Chem. B* 2021, 125, 10335−10343

Read Online

ACCESS | Metrics & More | Article Recommendations

ABSTRACT: Understanding the role of polymers rich in aspartic acid (Asp) and glutamic acid (Glu) is the key to gaining precise control over mineralization processes. Despite their chemical similarity, experiments revealed a surprisingly different influence of Asp and Glu sequences. We conducted molecular dynamics simulations of Asp and Glu peptides in the presence of calcium and chloride ions to elucidate the underlying phenomena. In line with experimental differences, in our simulations, we indeed find strong differences in the way the peptides interact with ions in solution. The investigated Asp pentapeptide tends to pull a lot of ions into its vicinity, and many structures with clusters of calcium and chloride ions on the surface of the peptide can be observed. Under the same conditions, comparatively fewer ions can be found in proximity of the investigated Glu pentapeptide, and the structures are characterized by single calcium ions bound to multiple carboxylate groups. Based on our simulation data, we identified three reasons contributing to these differences, leading to a new level of understanding additive−ion interactions.

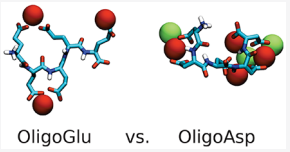

INTRODUCTION

Understanding the role of additives in mineralization processes is crucial to designing tailored materials with properties that could massively outperform simple, pure mineral phases.[1] Several examples from nature demonstrate the enormous potential that a sophisticated control of mineralization processes can provide.[2−4]

Analyzing how additives affect mineralization processes in biological or artificial systems, however, is a challenging task, because influences can occur in various stages of the mineralization process. This involves interactions with crystal surfaces on a millimeter scale but also interactions with tiny nuclei or crystal precursors on an Ångström scale.[5−7] Especially getting atomic/molecular insights into the early stages of mineralization is difficult through experimentation, though the multiple roles that additives can play in influencing mineralization processes have become more and more apparent.[8−11] Molecular dynamics simulation turned out to be a valuable tool to elucidate this gap.[12−17]

It has been known for some time that, for example, various calcium-carbonate-containing biominerals contain proteins rich in aspartic and glutamic acid.[18] The negatively charged carboxylate groups of these amino acids can strongly bind to the positively charged calcium ions, and it is therefore not surprising that an influence exists. Indeed, polycarboxylates are commonly employed in biomimetic mineralization studies,[19] and for instance, their presence is required for the in vitro mineralization of collagen as in bone.[20,21] While polycarboxylates stabilize so-called polymer-induced liquid precursors (PILPs),[19] the atomistic details of the mechanisms behind this influence of polycarboxylates remains an open question. This is especially the case since despite the similar chemical nature, aspartic acid and glutamic acid sequences appear to have a very different influence on mineralization processes. In the above-mentioned study of biomimetic collagen mineralization, for instance, polyaspartic acid facilitates intrafibrillar mineralization, while polyglutamic acid does not.[20] Especially, polyaspartic acid in solution is known to have a strong inhibiting or delaying effect on crystallization. It was shown to stabilize a liquid calcium carbonate precursor phase[22,23] and an amorphous phase in the case of calcium phosphate.[24] Polyglutamic acid was found to have only a weak crystallization inhibiting effect compared to polyaspartic acid.[25−27] These results indicate that already in the early stages during the formation of Ca minerals, glutamic-acid- and aspartic-acid-rich additives interact differently with the species in solution.

To gain further insights into the influences of glutamic acid and aspartic acid sequences on the early stages of mineralization, we conducted molecular dynamics simulations of penta-aspartic acid (pentaAsp) and pentaglutamic acid

Received: May 20, 2021
Revised: August 3, 2021
Published: September 2, 2021

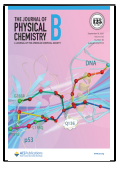

(pentaGlu) peptides in the presence of calcium and chloride ions. The analysis of pentamers allows to focus on local effects of a few neighboring functional groups, where conformational preferences in the peptides themselves are not pronounced. Long glutamic acid oligomers are for example known to have a strong tendency to form helices.[28] Choosing chloride as a counterion over the biologically more relevant but also more complex carbonate, phosphate, or oxalate ions allows focus upon the very basic interaction mechanisms of the additives.

In our simulations, we indeed found qualitative differences between the glutamic and aspartic acid oligomers. In a nutshell, we observed that pentaAsp tends to pull more calcium and chloride ions into its vicinity compared to pentaGlu. On the surface of pentaAsp, we often found clusters of calcium and chloride ions, while under the same conditions in the case of pentaGlu, we mainly found single calcium ions bound to one to three carboxylate groups. In the Results and Discussion, we provide a thorough analysis of these differences found in the simulation data. In the following, we describe our main conclusions up front, as they will guide us through the rest of the text.

The observations in our simulations lead us to propose three reasons that could lie behind or contribute to the different influence of aspartic and glutamic acid oligomers on the early stages of Ca-mineral formation. The three reasons are illustrated in Figure 1.

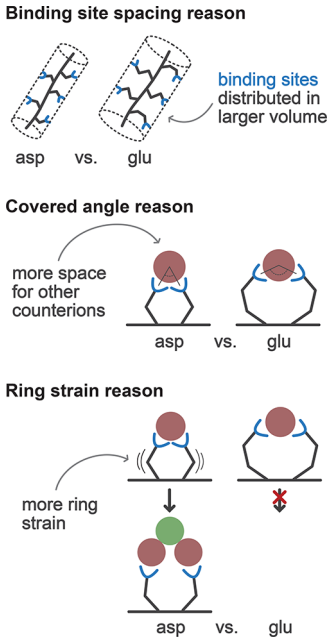

Figure 1. Illustrations of three potential reasons for the different influence of aspartic acid and glutamic acid sequences on mineralization processes.

(I) The "binding site spacing reason": In a very crude approximation, we can imagine both oligomers as a cylinder with a radius equal to the length of a side chain and a height equal to the length of the backbone. This cylinder roughly represents the volume in which the binding sites (carboxylate groups) are distributed. In comparison to oligoGlu, this imaginary cylinder is smaller in the case of oligoAsp because of the shorter side chains. OligoAsp, therefore, offers a higher density of binding sites. A higher density of negatively charged binding sites comes along with a higher charge density, which promotes the binding of counterions. In studies of simple-cylinder-like polyelectrolyte models, it was found that a certain critical charge density is required for counterions to be associated.[29,30] Once bound, a higher density of binding sites also tends to bring bound ions closer together and promotes the formation of ion clusters. In the case of oligoGlu, on the other hand, calcium ions associated with the binding sites are distributed in a larger volume and are therefore more likely to stay isolated from each other.

(II) The "covered angle reason": As it takes two negatively charged carboxylate groups to neutralize the two positive charges of calcium ions, two neighboring carboxylates bound to one calcium ion is a motif that often appears in our simulations. Due to the shorter length of the aspartic acid side chains, the geometry of the association of the two neighboring carboxylates at the ion is such that the two neighboring carboxylates cover a small angle of the calcium ion in this motif. There is still a lot of space for other counterions to approach the calcium ion, which facilitates cluster formation. With its longer side chains, on the other hand, two neighboring oligoGlu carboxylates can cover a wider angle of the calcium ion and shield it from other counterions.

(III) The "ring strain reason": There is a second effect of the side-chain length on the ring that is formed if two neighboring side-chain carboxylates are bound to the same calcium ion. In the case of the shorter aspartic acid side chain, this ring is strained, and in consequence, this motif is less favored compared to oligoGlu. In the case of oligoAsp, it is therefore more likely for one of the carboxylates to detach and to bind to a second calcium ion. This brings two calcium ions in close proximity and promotes the formation of clusters. On the other hand, in the case of oligoGlu this ring motif is comparatively stable and inhibits cluster formation.

Note that we focused our analysis on local aspects. Especially for longer chains, there might be further contributions to a different behavior of glutamic acid and aspartic acid sequences, e.g., due to conformational preferences of the peptides themselves.

Apart from simulations of pentamers in the presence of calcium and chloride ions, we also performed simulations of dimers in the presence of just a single calcium ion to corroborate the above-mentioned hypotheses. Plain molecular dynamics simulations of ion peptide systems struggle from slow sampling. The strong ion bridges formed can easily lock the peptide in one conformation for the rest of the simulation. To circumvent this problem and to obtain a broad sampling of possible conformations within the accessible time scales of a simulation, enhanced sampling techniques are required. In the case of the pentamer simulations, we used a Hamiltonian replica exchange,[31,32] and in the case of the dimer simulations, we used metadynamics.[33−35]

To get an overview of the sampled structures, we relied on the dimensionality reduction technique EncoderMap.[36,37] EncoderMap is a nonlinear dimensionality reduction technique that combines multidimensional scaling with a neural network autoencoder and is well-suited to generate meaningful maps of the conformational space.

https://doi.org/10.1021/acs.jpcb.1c04467
J. Phys. Chem. B 2021, 125, 10335−10343

In the following, we provide the computational details for the used simulation and analysis techniques before we discuss the results that lead us to the above-mentioned reasons.

COMPUTATIONAL DETAILS

Pentamer Simulations. Each simulated system consists of 1 pentapeptide, 10 calcium ions, 15 chloride ions, and 3538 water molecules. In principle, this reflects a 0.155 M solution of calcium ions. However, the concentration in such a small simulation volume is not directly comparable to a macroscopic concentration, because in a macroscopic system, the concentration might vary depending on the proximity to an additive molecule. All peptide carboxylic acid groups were simulated in the deprotonated state, and the terminal amino group was simulated in the protonated state. Together with the chosen number of calcium and chloride ions, this adds up to a neutral charge.

To run the simulations, the Gromacs 4.6.7 simulation package[38,39] was used with a modified version of the GROMOS 54A7[40] force field and the SPC/E water model.[41] The force field was modified regarding the calcium−oxygen Lennard-Jones parameters, to accurately represent the interactions between calcium ions and the carboxylate oxygen atoms in the glutamate and aspartate side chains. The original force field parameters were replaced with the values shown in Table 1, which were determined following the methods described in ref 42. The parameters were tuned to match experimental association constants of calcium and carboxylate groups as well as reference data from first-principles molecular dynamics simulations.

Table 1. Lennard-Jones Parameters for the Calcium−Oxygen Interaction

	C_6 [kJ nm^6 mol^{-1}]	C_{12} [kJ nm^{12} mol^{-1}]
GROMOS 54A7	0.00150765	2.16509×10^{-06}
used parameters	0.00203533	1.53721×10^{-06}

A combined Hamiltonian/temperature replica exchange setup was used to achieve an extensive sampling. For each pentapeptide, eight replicas were simulated for 1 μs each, resulting in a total simulated time of 8 μs for each system. The PLUMED2.1-hrex[43] plug-in for Gromacs was used to make the Hamiltonian replica exchange. The Hamiltonian of the different replicas was altered with a set of parameter changes described in reference 44, which was designed to facilitate the sampling of ion−peptide systems. This involves biased backbone dihedral torsions to enhance the flexibility of the backbone, altered Ca−O interactions to weaken ion bridges, and increased temperature to promote the diffusion of ions. Table 2 summarizes the changed parameters in the different replicas. Replica 0 in this setup corresponds to the unchanged Hamiltonian, and all results shown later are derived from this unchanged replica.

The temperature was kept constant during the simulation using stochastic velocity rescaling by Bussi et al.[45] The pressure was not readjusted during the main simulations. In preceding equilibration simulations, a Berendsen barostat[46] was used to bring the simulation to 1 bar. The leapfrog algorithm with a time step of 2 fs was used to integrate the equations of motion. Long range interactions were calculated with the particle mesh Ewald method[47] with a grid spacing of 0.12 nm and an pme-order of 4. Both Coulomb and Lennard-Jones interactions were truncated at 1.4 nm. Bonds have been constrained using the linear constraints solver (LINCS) algorithm[48] with an eighth-order expansion.

Table 2. Parameters That Were Varied in the Hamiltonian Replica Exchange Simulations[a]

replica	T [K]	α	C_6 [kJ nm^6 mol^{-1}]	C_{12} [kJ nm^{12} mol^{-1}]
7	310.5	−1.00	1.88×10^{-03}	1.72×10^{-06}
6	309.0	−0.86	1.91×10^{-03}	1.69×10^{-06}
5	307.5	−0.71	1.93×10^{-03}	1.67×10^{-06}
4	306.0	−0.57	1.95×10^{-03}	1.64×10^{-06}
3	304.5	−0.43	1.97×10^{-03}	1.61×10^{-06}
2	303.0	−0.29	1.99×10^{-03}	1.59×10^{-06}
1	301.5	−0.14	2.01×10^{-03}	1.56×10^{-06}
0	300.0	0.0	2.04×10^{-03}	1.54×10^{-06}

[a] T denotes the temperature of the given replica. α is a prefactor that adjusts the strength of the biasing potential on the backbone dihedral torsions. C_6 and C_{12} are Lennard-Jones parameters of the Ca−O interaction. See reference 44 for more details.

Dimer Simulations. The dimer simulations contain 1 glutamate or aspartate dimer where the end groups were capped with an *N*-methyl and an acetyl group respectively, 1 calcium ion, and 2500 water molecules. All simulation settings and force field parameters were chosen equivalently to the pentamer simulations. We used metadynamics to calculate potentials of mean force of ion association, i.e., the free energy as a function of the distance of the calcium ion to the two carboxylate groups. To take advantage of the symmetry of the problem and to facilitate the interpretation, we only show the results of one-dimensional metadynamics runs, where the side-chain carboxylate group at the N-terminus was kept in contact with the calcium ion by applying a harmonic upper wall potential to the calcium ↔ carboxylate-carbon distance with a force constant of 100 000 $\frac{\text{kJ}}{\text{mol}\cdot\text{nm}^2}$ at a distance of 0.32 nm. Well tempered metadynamics was performed with the distance between the calcium ion and the C-terminal side-chain carboxylate-carbon atom as collective variable. Every picosecond, Gaussians with a sigma of 0.005 nm, an initial height of 0.5 $\frac{\text{kJ}}{\text{mol}}$, and a bias factor of 5 were added to the history-dependent biasing potential. This one-dimensional approach where the ion is restrained in contact with one of the carboxylates allows to thoroughly map out a slice of the two-dimensional free energy landscape with both calcium carboxylate distances as collective variables. Gromacs 2019.3[49] was used to run the simulations, and the PLUMED2.5.2 plugin[50] was used for the metadynamics.

EncoderMap Projections. Two-dimensional maps of the pentamer simulation data were created using EncoderMap.[36,37] All pairwise distances (in nanometers) between the side-chain carboxylic acid carbon atoms were used as input space for the dimensionality reduction. The used autoencoder with tanh activation functions consisted of 2 layers of 128 neurons, a bottleneck layer with 2 neurons, and another 2 layers with 128 neurons. The weights in the network were optimized to minimize EncoderMap's cost function with an autocost-scale of 1 and a distance-cost-scale of 500. The used parameters for the sigmoid functions used in the distance-based part of the cost function are σ = 0.5, a = 5, and b = 5 for the high-dimensional distances and σ = 1, a = 5, and b = 5 for the low-dimensional distances. The optimization was done in 50 000 steps with batches of 256 data points, a learning rate of 0.001,

https://doi.org/10.1021/acs.jpcb.1c04467
J. Phys. Chem. B 2021, 125, 10335−10343

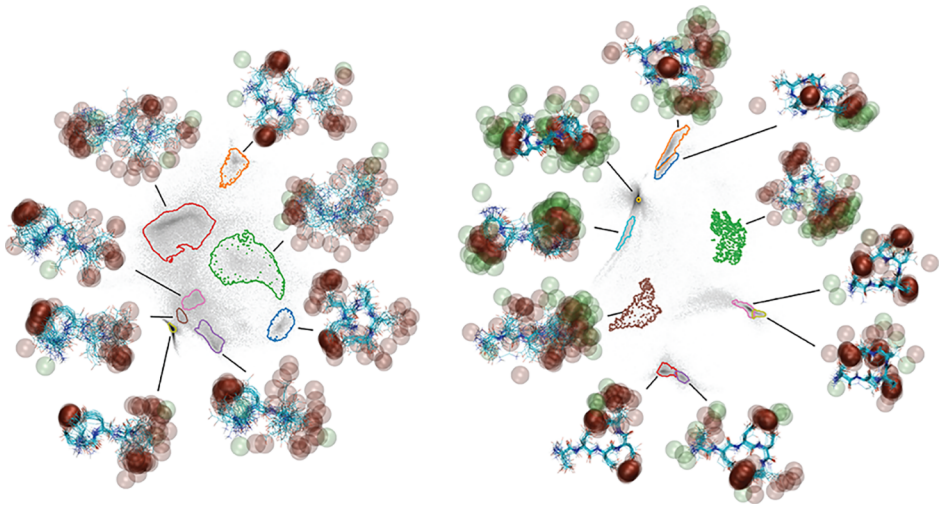

Figure 2. Conformational maps obtained with EncoderMap of pentaGlu (left) and pentaAsp (right). The density of points (each representing a peptide conformation) is shown in these 2D-histograms on a logarithmic gray scale (dark = high density). The color-coded areas in the map represent clusters identified with the HDBSCAN clustering algorithm.[51] Next to the clusters, 25 overlaid structures from the corresponding clusters are shown. Ions are shown in semitransparent to give an impression where ions are often present and where they are present only in few of the structures.

and an l2 regularization constant of 0.001. In the resulting two-dimensional projections, clusters where identified using HDBSCAN with the leaf cluster selection method.[51] In the case of pentaAsp, a minimum cluster size of 1000 and a minimum number of 50 samples in a neighborhood for a point to be considered a core point were chosen. In the case of pentaGlu, a minimum cluster size of 1500 and a minimum number of 500 samples were chosen.

RESULTS AND DISCUSSION

We performed extensive molecular dynamics simulations of pentaAsp and pentaGlu in the presence of calcium and chloride ions in water. First, we will show the differences in the structural ensembles sampled by the two peptide−ion systems. To this end, we used the dimensionality reduction method EncoderMap to generate a two-dimensional representation of the respective conformational spaces, into which all simulated structures were projected. In the low-dimensional representation, each conformation is represented with a point, and the locations of these points are optimized in such a way that the distances between the low-dimensional points reflect the distances between the corresponding conformations in the high-dimensional descriptor space. Consequently, similar conformations are represented by points that are in close proximity in the 2D-projection.

We chose all pairwise distances between the carboxylate-carbon atoms as the high-dimensional descriptor for the dimensionality reduction, because this descriptor focuses on the ion binding site positions. Figure 2 shows 2D-histograms of the obtained 2D-projections of the pentaGlu and pentaAsp data. Clusters in the projections were identified using HDBSCAN.[51] Next to each cluster, 25 superimposed conformations from the corresponding cluster are shown, including the ions within 0.4 nm of any peptide atom. The calcium and chloride ions are shown in transparent red and green, respectively. Saturated regions in the ion cloud therefore represent positions where ions are present in most or all cluster conformations.

In the case of pentaGlu, besides few exceptions, no chloride ions are present in the vicinity of the peptide. From the dense red spots in the shown ion clouds, we can identify single calcium ions connecting pairs of carboxylates (e.g., in the orange and blue clusters). There are also structures where three carboxylate groups are linked by a single calcium ion (bottom left corner of the map).

In contrast, in the case of the pentaAsp structures shown in Figure 2 on the right, there are plenty of chloride ions visible in the vicinity of the peptide. Here, we can also find several structures with single calcium ions connecting two carboxylate groups (e.g., in the red, purple, and pink clusters), but there are also clusters with dense ion clouds (top left corner) that indicate the presence of multiple calcium and chloride ions grouped together.

Despite the similarity of pentaAsp and pentaGlu, already the rough overview of sampled structures provided by the dimensionality reduction and clustering analysis provides a visual impression of the large differences in the interplay with ions. To quantify this difference, we counted the number of calcium and chloride ions within 0.4 nm of the respective peptide in each frame of the simulations. The results are shown in the histograms in Figure 3.

Two is the most common number of calcium ions found in the proximity of pentaGlu, and in more than 80% of the simulation frames, no chloride ions were present in the vicinity of pentaGlu. In case of pentaAsp, three to four calcium ions can usually be found in the vicinity, and two is the most likely number of chloride ions present. In the bottom of Figure 3, two example structures are shown that reflect the most likely scenarios.

Figures 2 and 3 show clear differences between pentaAsp and pentaGlu, but further analysis was necessary to rationalize and interpret them. For some well-defined clusters, the ion bridge patterns are already nicely visible in Figure 2, but for some of the more diverse clusters, it is difficult to recognize the ion bridges present. To get a better insight into the different ion bridge patterns, we developed a simplified representation illustrated in Figure 4. In this representation, the peptide is

https://doi.org/10.1021/acs.jpcb.1c04467
J. Phys. Chem. B 2021, 125, 10335−10343

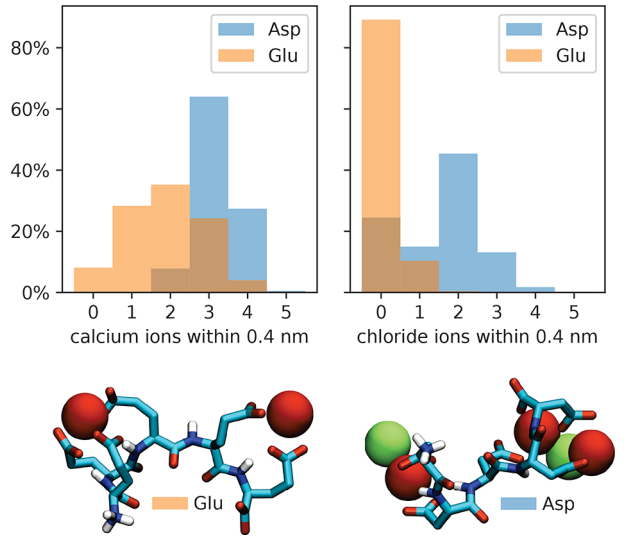

Figure 3. Number of ions present in the proximity of pentaGlu (orange histograms) and pentaAsp (blue histograms). The left graph shows the fraction of simulation frames where the number of calcium ions given on the *x*-axis is present within 0.4 nm of any peptide atom. The right graph shows the results for the equivalent analysis with chloride ions.

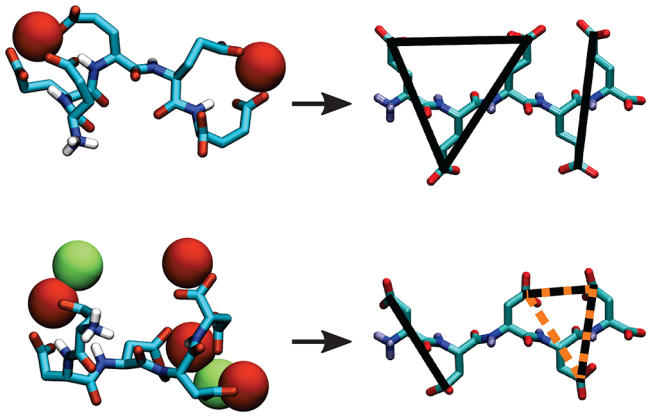

Figure 4. Ion bridge pattern analysis. The two representations on the right show the ion bridges identified for the two example structures shown on the left. "Direct" ion bridges, i.e., pairs of carboxylates bound to the same calcium ion, are marked with a black line. "Indirect" ion bridges, i.e., pairs of carboxylates connected through two calcium ions and a chloride ion, are marked with a dashed orange line.

always shown in an extended conformation, and pairs of carboxylates bound to the same calcium ion are marked with a connecting black line. In this analysis, carboxylates are considered to be bound to a calcium ion if the distance between the centers of the carboxylate C atom and the calcium ion is smaller than 0.4 nm. Besides these "direct" ion bridges, also "indirect" ion bridges play a role, where carboxylates are connected through two calcium ions and a chloride ion. Figure 4 on the bottom shows an example for such an indirect ion bridge that is marked with a dashed orange line in the simplified representation. In some cases, two carboxylates are both in contact with the same calcium ion, and they are simultaneously also linked through an indirect ion bridge. In those cases, a black line and an orange dashed line are shown.

Figures 5 and 6 show the 10 most populated ion bridge connection patterns for pentaGlu and pentaAsp, respectively. For reference, also the EncoderMap projections from Figure 2 are shown colored according to the ion bridge connection patterns. In the case of pentaGlu, we can find several structures with just one bridged pair of carboxylates. Even structures with no bridged carboxylates (green) are quite common. In the case of pentaGlu, we can also only find direct ion bridges; no indirect bridges where carboxylates are linked by two calcium ions and a chloride ion are present among the 10 most common ion bridge patterns.

In case of pentaAsp, all of the ten most common ion bridge connection patterns have at least two connections. Besides direct ion bridges, also indirect ion bridges are present in many of the pentaAsp connection patterns.

These structural findings can be interpreted now in the context of the three reasons proposed in the introduction. The scarcity of ion bridges in the case of pentaGlu is nicely in line with the "binding site spacing reason". The space available to the pentaGlu carboxylates is comparatively large, which reduces the probability of bridged carboxylates. The large number of indirect ion bridges in the case of pentaAsp supports the "ring strain reason". If the small ring created by two neighboring carboxylates connected to the same calcium ion is strained, it drives the system toward larger, less-strained rings. The system can thus avoid ring strain by forming more indirect ion bridges, where neighboring carboxylates are bound to two calcium ions and a chloride ion in a comparatively large ring.

To further investigate the "ring strain reason", we performed simulations of aspartic and glutamic acid dimers in the presence of just one calcium ion. To avoid a strong influence of the end groups and to imitate the situation in a longer chain, the ends were capped with an *N*-methyl and an acetyl group, respectively. Consequently, in these systems, just one ring is possible, which allows focus on this motif. Different factors can contribute to the mean force that represents such a ring strain, such as energetic contributions through unfavorably twisted angles or torsions but also entropic contributions, e.g., due to limiting the accessible conformational space of the side chains or due to trapping or releasing solvent molecules. To capture all these contributions, we used metadynamics simulations to calculate the free energy as a function of the distance of the calcium ion to one carboxylate group while remaining bound to the second carboxylate group. In other words, we forced the calcium ion to stay in contact with one of the carboxylate groups by applying a restraining potential, while we extracted the free energy as a function of the distance to the other carboxylate group. Figure 7 shows the resulting free energy profiles.

Both free energy profiles have their global minimum just below 0.3 nm, which corresponds to a bidentate/bidentate state, i.e., both carboxylates are in contact to the calcium ion with both their oxygen atoms. Both free energy profiles were aligned at this minimum. The next minimum (around 0.35 nm) corresponds to a bidentate/monodentate state, i.e., the carboxylate that is not forced to stay in the bidentate state has contact to the calcium ion only through one of its oxygen atoms. The third minimum (0.5 to 0.6 nm) corresponds to a bidentate/solvent-shared state, i.e., the free carboxylate group is separated by one layer of water molecules from the calcium ion. Both the bidentate/monodentate and the bidentate/solvent-shared states have a lower free energy in the case of the

https://doi.org/10.1021/acs.jpcb.1c04467
J. Phys. Chem. B 2021, 125, 10335−10343

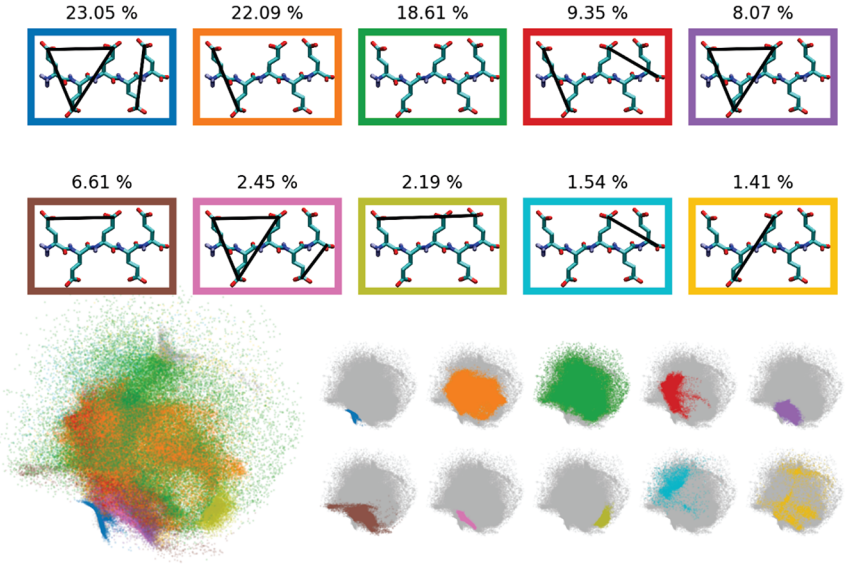

Figure 5. PentaGlu ion bridge patterns. In the colored boxes, the 10 most common ion bridge patterns of the pentaGlu simulation are shown. The numbers above each box provide the fraction of frames in which the respective pattern is occurring. In the bottom, the EncoderMap projection from Figure 2 is shown colored according to the ion bridge pattern. In the large map on the left, all patterns are colored. In the smaller maps in the bottom right, only one pattern is colored in each copy of the map for better visibility.

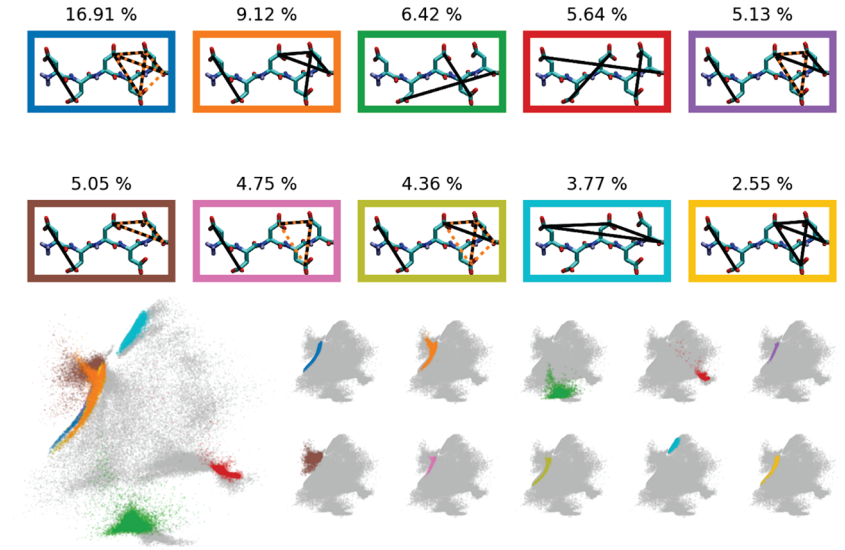

Figure 6. PentaAsp ion bridge patterns. In the colored boxes, the 10 most common ion bridge patterns of the pentaAsp simulation are shown. The numbers above each box provide the fraction of frames in which the respective pattern is occurring. In the bottom, the EncoderMap projection from Figure 2 is shown colored according to the ion bridge pattern. In the large map on the left, all patterns are colored. In the smaller maps in the bottom right, only one pattern is colored in each copy of the map for better visibility.

aspartic acid dimer compared to the glutamic acid dimer. This strongly supports the "ring strain reason". In the case of the aspartic acid dimer, the bidentate/bidentate state requires a strained ring, and therefore, the system is more likely to evade into a less-strained monodentate or solvent-shared state compared to the glutamic acid system.

To analyze the impact of this ring motif in longer peptide sequences, we analyzed the distances between neighboring carboxylates in the pentapeptide simulations. The histograms in Figure 8 show how frequently certain distances between neighboring carboxylate-carbon atoms occur, i.e., the histograms comprise the distances of the first to the second, the second to the third, the third to the fourth, etc. carboxylate C atom along the chain. Both histograms are normalized to an integral of 1.

In the case of pentaGlu, long neighbor distances are frequently occurring in a range (>0.85 nm) that is not accessible for the pentaAsp system. This again emphasizes the "binding site spacing reason".

For the short distances (around 0.4 nm), we can see a sharp peak in both distributions. In the case of pentaAsp, this peak is shifted to smaller distances compared to pentaGlu. Further analysis of the structures behind these peaks (neighbor carboxylate-carbon distances of 0.5 nm in the case of pentaGlu and 0.44 nm in the case of pentaAsp) revealed that in 91% of the cases bidentate/bidentate states (all four oxygen atoms within 0.3 nm of the same calcium ion) are responsible for

https://doi.org/10.1021/acs.jpcb.1c04467
J. Phys. Chem. B 2021, 125, 10335−10343

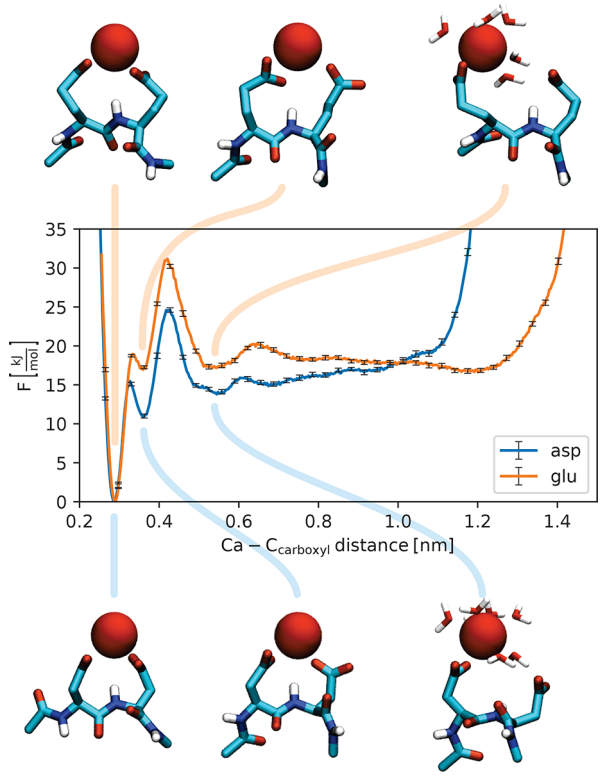

Figure 7. Free energy analysis of the ring motive. The graph shows the free energy as a function of the distance between the calcium ion and the C-terminal side-chain carboxylate-carbon atom, while the calcium ion was forced to stay in contact with the N-terminal carboxylate of a glutamate/aspartate dimer. The structures above and below the graph show example snapshots for the marked distances. The error bars indicate the standard error of the mean obtained by block averaging (after unbiasing, see ref 52) of ten 100 ns trajectory blocks.

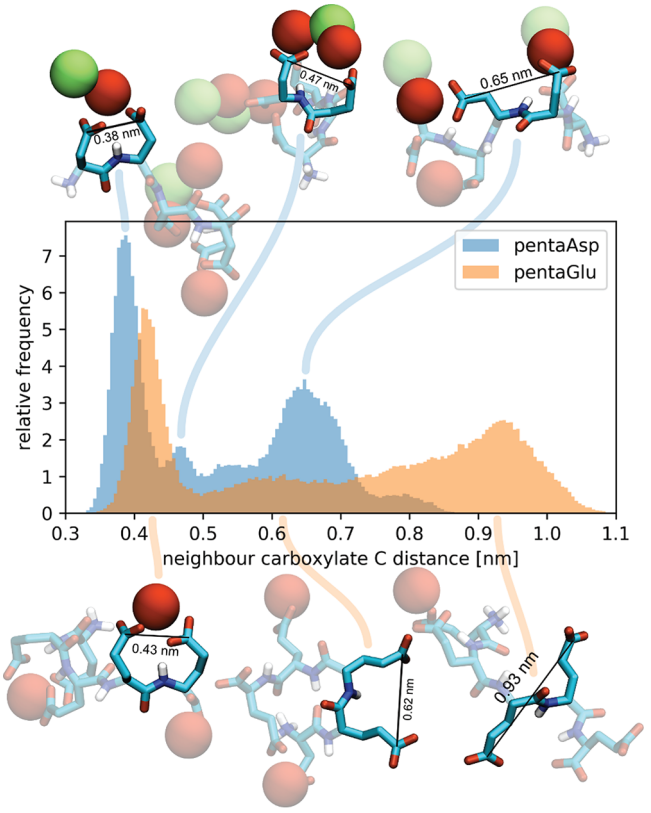

Figure 8. Distance distributions of neighboring carboxylate-carbon atoms. These histograms combine the distances between all neighboring pairs of carboxylates along the chain from the pentaGlu and pentaAsp simulations. The snapshots above and below the histograms show example structures for relevant distances for pentaAsp and pentaGlu, respectively.

these distances, both in the case of pentaGlu and pentaAsp. This demonstrates that these highest peaks in the histograms essentially correspond to the lowest minima in the free energy profiles in Figure 7. The shift of the two peaks shows that in the case of pentaAsp the carboxylates are closer together in the bidentate/bidentate state compared to pentaGlu, which supports the "covered angle reason". Neighboring carboxylates bound to the same calcium ion are located more on one side of the calcium ion and only cover a smaller angle of the calcium ion. Consequently, more surface of the calcium ion is still accessible for other counterions. To verify that the covered angle is indeed different, we computed the carboxylate-carbon/calcium/carboxylate-carbon angle for all structures with a bidentate/bidentate motif within the two peaks (i.e., for regions with neighboring carboxylate C distances of 0.5 nm in the case of pentaGlu and 0.44 nm in the case of pentaAsp). With 83.4°, the obtained average carboxylate-carbon/calcium/carboxylate-carbon angle is distinctly smaller in the case of pentaAsp compared to pentaGlu with 92.3°.

We can also see that the peak corresponding mainly to this bidentate/bidentate state is higher in the case of pentaAsp compared to pentaGlu. On first sight, this contradicts the "ring strain reason". If this state involves a strained ring, it should not be overly populated in the case of pentaAsp. However, there are two opposing effects at play here. The ring strain is an argument against a lot of direct ion bridges between neighboring carboxylates in the case of pentaAsp. At the same time, the "binding site spacing reason" is an argument against a lot of direct ion bridges between neighboring carboxylates in the case of pentaGlu, for entropic reasons. The height of the peak around 0.4 nm alone is therefore not conclusive.

In the range of 0.45 to 0.5 nm, there is a small peak in the case of pentaAsp that is not present in the case of pentaGlu. Distances between neighboring carboxylates bridged by two calcium ions and a counterion fall into this range as the corresponding snapshot in Figure 8 shows. A closer look at the snapshot reveals that indeed both carboxylates are bridged by two calcium ions, but at the same time, both carboxylates are attached to the calcium ion on the right in a bidentate/monodentate fashion. Consequently, this distance range is closely related to the second free energy minimum from the left in Figure 7. The low free energy of the bidentate/monodentate state in the case of diAsp is in good agreement with the comparatively high occurrence of the intermediate neighbor carboxylate-carbon distances (0.45 to 0.5 nm) in pentaAsp. This nicely demonstrates that the "ring strain reason" is not only relevant in the simple dimer system but also in longer chains.

With that, Figure 8 contains evidence for all three reasons proposed in the introduction, which highlights that the differences in behavior can not be attributed to a single reason but indeed to a complex interplay of multiple contributions. In experimental setups, the picture can be even more complex. If

https://doi.org/10.1021/acs.jpcb.1c04467
J. Phys. Chem. B 2021, 125, 10335−10343

long polycarboxylate chains are used, folding might play a role, and additionally to rings formed between neighboring carboxylates, bridges between different segments of the chain might become important. Also, interactions between multiple chains might play a role especially in systems with high polycarboxylate concentrations, and a possible phase separation into liquid precursor states further complicates the situation. Despite these issues, which make a direct comparison of our simulation results to experimental data very difficult, the stronger tendency of pentaAsp to bind ions, found in our simulations, is nicely in line with the stronger effect of aspartate additives on the mineralization processes compared to glutamate additives that is reported in the literature.[20] In addition, also for uncapped single amino acids, ion effects were observed experimentally[53]—but only at large concentrations. It is however difficult to interpret these results in the context of the present work, since on the one hand, monomer systems are dominated by end group effects, and on the other hand, the effects due to interactions between neighboring side chains (e.g., ring motifs) cannot occur.

CONCLUSION

Our simulations show that aspartic acid and glutamic acid sequences have a very different influence on ions in solution. The simulated pentaAsp peptide tends to pull more calcium and counterions into its vicinity compared to pentaGlu and induces the formation of ion clusters on its surface. In our simulation studies, we have identified three potential reasons that could explain this different influence of aspartic acid and glutamic acid sequences: the "binding site spacing reason", the "covered angle reason", and the "ring strain reason". While we derived these reasons from simulations of systems with oligopeptides in the presence of calcium and chloride ions and while a quantitative comparison to experiments is difficult, we are convinced that the underlying concepts are so fundamental that they can be transferred to other systems. Thus, they can serve as a basis to interpret experimental observations where glutamic-acid- and aspartic-acid-rich peptides affect calcium carbonate, phosphate, or oxalate mineralization. The current developments in ab initio methods and sophisticated force fields derived from the former (e.g., through machine learning) provide good prospects to get further insights on a more quantitative level and into more subtle effects in the future.

AUTHOR INFORMATION

Corresponding Author

Christine Peter − *Theoretical Chemistry, University of Konstanz, 78547 Konstanz, Germany;* orcid.org/0000-0002-1471-5440; Email: Christine.Peter@uni-konstanz.de

Authors

Tobias Lemke − *Theoretical Chemistry, University of Konstanz, 78547 Konstanz, Germany;* orcid.org/0000-0002-0593-2304

Moritz Edte − *Theoretical Chemistry, University of Konstanz, 78547 Konstanz, Germany*

Denis Gebauer − *Institute of Inorganic Chemistry, Leibniz University Hannover, 30167 Hannover, Germany;* orcid.org/0000-0003-1612-051X

Complete contact information is available at: https://pubs.acs.org/10.1021/acs.jpcb.1c04467

Notes

The authors declare no competing financial interest.

ACKNOWLEDGMENTS

We thank Christoph Globisch and Nicolas Schneider for proofreading and for very helpful feedback. We thank Maxim Gindele for valuable discussions regarding the experimental background. We gratefully acknowledge funding by the German Research Foundation (DFG) through SFB1214. The authors acknowledge support by the state of Baden-Württemberg through bwHPC and the DFG through grant INST 37/935-1 FUGG.

REFERENCES

(1) Nudelman, F.; Sommerdijk, N. A. Biomineralization as an inspiration for materials chemistry. *Angew. Chem., Int. Ed.* **2012**, *51*, 6582−6596.

(2) Politi, Y.; Arad, T.; Klein, E.; Weiner, S.; Addadi, L. Sea urchin spine calcite forms via a transient amorphous calcium carbonate phase. *Science* **2004**, *306*, 1161−1164.

(3) Addadi, L.; Joester, D.; Nudelman, F.; Weiner, S. Mollusk shell formation: a source of new concepts for understanding biomineralization processes. *Chem. - Eur. J.* **2006**, *12*, 980−987.

(4) Aizenberg, J.; Weaver, J. C.; Thanawala, M. S.; Sundar, V. C.; Morse, D. E.; Fratzl, P. Skeleton of Euplectella sp.: structural hierarchy from the nanoscale to the macroscale. *Science* **2005**, *309*, 275−278.

(5) Meldrum, F. C.; Cölfen, H. Controlling mineral morphologies and structures in biological and synthetic systems. *Chem. Rev.* **2008**, *108*, 4332−4432.

(6) Gebauer, D.; Cölfen, H. Prenucleation clusters and non-classical nucleation. *Nano Today* **2011**, *6*, 564−584.

(7) Shtukenberg, A. G.; Ward, M. D.; Kahr, B. Crystal growth with macromolecular additives. *Chem. Rev.* **2017**, *117*, 14042−14090.

(8) Gebauer, D. How can additives control the early stages of mineralisation? *Minerals* **2018**, *8*, 179.

(9) Gebauer, D.; Cölfen, H.; Verch, A.; Antonietti, M. The multiple roles of additives in CaCO3 crystallization: A quantitative case study. *Adv. Mater.* **2009**, *21*, 435−439.

(10) Segman-Magidovich, S.; Rapaport, H. The effects of template rigidity and amino acid type on heterogeneous calcium-phosphate mineralization by Langmuir films of amphiphilic and acidic β-sheet peptides. *J. Phys. Chem. B* **2012**, *116*, 11197−11204.

(11) Sun, C. C.; Sun, W.; Price, S.; Hughes, C.; Ter Horst, J.; Veesler, S.; Lewtas, K.; Myerson, A.; Pan, H.; Coquerel, G.; et al. Solvent and additive interactions as determinants in the nucleation pathway: general discussion. *Faraday Discuss.* **2015**, *179*, 383−420.

(12) Wallace, A. F.; Hedges, L. O.; Fernandez-Martinez, A.; Raiteri, P.; Gale, J. D.; Waychunas, G. A.; Whitelam, S.; Banfield, J. F.; De Yoreo, J. J. Microscopic evidence for liquid-liquid separation in supersaturated CaCO3 solutions. *Science* **2013**, *341*, 885−889.

(13) Demichelis, R.; Raiteri, P.; Gale, J. D.; Quigley, D.; Gebauer, D. Stable prenucleation mineral clusters are liquid-like ionic polymers. *Nat. Commun.* **2011**, *2*, 590.

(14) Kahlen, J.; Peter, C.; Donadio, D. Molecular simulation of oligo-glutamates in a calcium-rich aqueous solution: insights into peptide-induced polymorph selection. *CrystEngComm* **2015**, *17*, 6863−6867.

(15) Jain, A.; Jochum, M.; Peter, C. Molecular Dynamics Simulations of Peptides at the Air-Water Interface: Influencing Factors on Peptide-Templated Mineralization. *Langmuir* **2014**, *30*, 15486−15495.

(16) Tolmachev, D.; Lukasheva, N.; Mamistvalov, G.; Karttunen, M. Influence of Calcium Binding on Conformations and Motions of Anionic Polyamino Acids. Effect of Side Chain Length. *Polymers* **2020**, *12*, 1279.

(17) Xu, Z.; Wei, Q.; Zhao, W.; Cui, Q.; Sahai, N. Essence of small molecule-mediated control of hydroxyapatite growth: free energy calculations of amino acid side chain analogues. *J. Phys. Chem. C* **2018**, *122*, 4372−4380.
(18) Lowenstam, H. A.; Weiner, S.; et al. *On biomineralization*; Oxford University Press: New York, 1989.
(19) Gower, L. B. Biomimetic model systems for investigating the amorphous precursor pathway and its role in biomineralization. *Chem. Rev.* **2008**, *108*, 4551−4627.
(20) Thula, T. T.; Svedlund, F.; Rodriguez, D. E.; Podschun, J.; Pendi, L.; Gower, L. B. Mimicking the nanostructure of bone: comparison of polymeric process-directing agents. *Polymers* **2011**, *3*, 10−35.
(21) Nudelman, F.; Pieterse, K.; George, A.; Bomans, P. H.; Friedrich, H.; Brylka, L. J.; Hilbers, P. A.; de With, G.; Sommerdijk, N. A. The role of collagen in bone apatite formation in the presence of hydroxyapatite nucleation inhibitors. *Nat. Mater.* **2010**, *9*, 1004−1009.
(22) Gower, L. B.; Odom, D. J. Deposition of calcium carbonate films by a polymer-induced liquid-precursor (PILP) process. *J. Cryst. Growth* **2000**, *210*, 719−734.
(23) Bewernitz, M. A.; Gebauer, D.; Long, J.; Cölfen, H.; Gower, L. B. A metastable liquid precursor phase of calcium carbonate and its interactions with polyaspartate. *Faraday Discuss.* **2012**, *159*, 291−312.
(24) Cantaert, B.; Beniash, E.; Meldrum, F. C. The role of poly (aspartic acid) in the precipitation of calcium phosphate in confinement. *J. Mater. Chem. B* **2013**, *1*, 6586−6595.
(25) Jung, T.; Kim, W.-S.; Kyun Choi, C. Crystal structure and morphology control of calcium oxalate using biopolymeric additives in crystallization. *J. Cryst. Growth* **2005**, *279*, 154−162.
(26) Wesson, J. A.; Worcester, E. M.; Kleinman, J. G. Role of anionic proteins in kidney stone formation: interaction between model anionic polypeptides and calcium oxalate crystals. *J. Urol.* **2000**, *163*, 1343−1348.
(27) Guo, S.; Ward, M. D.; Wesson, J. A. Direct visualization of calcium oxalate monohydrate crystallization and dissolution with atomic force microscopy and the role of polymeric additives. *Langmuir* **2002**, *18*, 4284−4291.
(28) Hunkler, S.; Lemke, T.; Peter, C.; Kukharenko, O. Back-mapping based sampling: Coarse grained free energy landscapes as a guideline for atomistic exploration. *J. Chem. Phys.* **2019**, *151*, 154102.
(29) Manning, G. S. Polyelectrolytes. *Annu. Rev. Phys. Chem.* **1972**, *23*, 117−140.
(30) Heyda, J.; Dzubiella, J. Ion-specific counterion condensation on charged peptides: Poisson−Boltzmann vs. atomistic simulations. *Soft Matter* **2012**, *8*, 9338−9344.
(31) Sugita, Y.; Okamoto, Y. Replica-exchange molecular dynamics method for protein folding. *Chem. Phys. Lett.* **1999**, *314*, 141−151.
(32) Fukunishi, H.; Watanabe, O.; Takada, S. On the Hamiltonian replica exchange method for efficient sampling of biomolecular systems: Application to protein structure prediction. *J. Chem. Phys.* **2002**, *116*, 9058−9067.
(33) Huber, T.; Torda, A. E.; Van Gunsteren, W. F. Local elevation: a method for improving the searching properties of molecular dynamics simulation. *J. Comput.-Aided Mol. Des.* **1994**, *8*, 695−708.
(34) Grubmüller, H. Predicting slow structural transitions in macromolecular systems: Conformational flooding. *Phys. Rev. E: Stat. Phys., Plasmas, Fluids, Relat. Interdiscip. Top.* **1995**, *52*, 2893−2906.
(35) Barducci, A.; Bussi, G.; Parrinello, M. Well-tempered metadynamics: a smoothly converging and tunable free-energy method. *Phys. Rev. Lett.* **2008**, *100*, 020603.
(36) Lemke, T.; Peter, C. Encodermap: Dimensionality reduction and generation of molecule conformations. *J. Chem. Theory Comput.* **2019**, *15*, 1209−1215.
(37) Lemke, T.; Berg, A.; Jain, A.; Peter, C. EncoderMap (II): Visualizing important molecular motions with improved generation of protein conformations. *J. Chem. Inf. Model.* **2019**, *59*, 4550−4560.
(38) van der Spoel, D.; Lindahl, E.; Hess, B.; Groenhof, G.; Mark, A. E.; Berendsen, H. J. C. GROMACS: Fast, flexible, and free. *J. Comput. Chem.* **2005**, *26*, 1701−1718.
(39) Hess, B.; Kutzner, C.; van der Spoel, D.; Lindahl, E. GROMACS 4: Algorithms for Highly Efficient, Load-Balanced, and Scalable Molecular Simulation. *J. Chem. Theory Comput.* **2008**, *4*, 435−447.
(40) Schmid, N.; Eichenberger, A. P.; Choutko, A.; Riniker, S.; Winger, M.; Mark, A. E.; van Gunsteren, W. F. Definition and testing of the GROMOS force-field versions 54A7 and 54B7. *Eur. Biophys. J.* **2011**, *40*, 843−856.
(41) Berendsen, H. J. C.; Grigera, J. R.; Straatsma, T. P. The missing term in effective pair potentials. *J. Phys. Chem.* **1987**, *91*, 6269−6271.
(42) Kahlen, J.; Salimi, L.; Sulpizi, M.; Peter, C.; Donadio, D. Interaction of charged amino-acid side chains with ions: An optimization strategy for classical force fields. *J. Phys. Chem. B* **2014**, *118*, 3960−3972.
(43) Bussi, G. Hamiltonian replica exchange in GROMACS: a flexible implementation. *Mol. Phys.* **2014**, *112*, 379−384.
(44) Lemke, T.; Peter, C.; Kukharenko, O. Efficient Sampling and Characterization of Free Energy Landscapes of Ion-Peptide Systems. *J. Chem. Theory Comput.* **2018**, *14*, 5476−5488.
(45) Bussi, G.; Donadio, D.; Parrinello, M. Canonical sampling through velocity rescaling. *J. Chem. Phys.* **2007**, *126*, 014101.
(46) Berendsen, H. J. C.; Postma, J. P. M.; van Gunsteren, W. F.; DiNola, A.; Haak, J. R. Molecular dynamics with coupling to an external bath. *J. Chem. Phys.* **1984**, *81*, 3684−3690.
(47) Essmann, U.; Perera, L.; Berkowitz, M. L.; Darden, T.; Lee, H.; Pedersen, L. G. A smooth particle mesh Ewald method. *J. Chem. Phys.* **1995**, *103*, 8577−8593.
(48) Hess, B.; Bekker, H.; Berendsen, H. J. C.; Fraaije, J. G. E. M. LINCS: A linear constraint solver for molecular simulations. *J. Comput. Chem.* **1997**, *18*, 1463−1472.
(49) Abraham, M. J.; Murtola, T.; Schulz, R.; Páll, S.; Smith, J. C.; Hess, B.; Lindahl, E. GROMACS: High performance molecular simulations through multi-level parallelism from laptops to supercomputers. *SoftwareX* **2015**, *1*, 19−25.
(50) Tribello, G. A.; Bonomi, M.; Branduardi, D.; Camilloni, C.; Bussi, G. PLUMED 2: New feathers for an old bird. *Comput. Phys. Commun.* **2014**, *185*, 604−613.
(51) McInnes, L.; Healy, J.; Astels, S. hdbscan: Hierarchical density based clustering. *J. Open Source Softw.* **2017**, *2*, 205.
(52) Bussi, G.; Tribello, G. A. Analyzing and Biasing Simulations with PLUMED. *Methods Mol. Biol.* **2019**, *2022*, 529−578.
(53) Picker, A.; Kellermeier, M.; Seto, J.; Gebauer, D.; Cölfen, H. The multiple effects of amino acids on the early stages of calcium carbonate crystallization. *Z. Kristallogr. - Cryst. Mater.* **2012**, *227*, 744−757.

https://doi.org/10.1021/acs.jpcb.1c04467
J. Phys. Chem. B 2021, 125, 10335−10343